Sound & Vibration 2026, 60(3), 3981.
doi: https://doi.org/10.59400/sv3981

Article

Mathematical and numerical modeling of resonant frequencies of fluid-structure systems for digital twins

Bauyrzhan Amirkhanov[1*], Gulshat Amirkhanova[1], Murat Kunelbayev[1,2], Alina Raeva[1]

[1] Department of Artificial Intelligence and Big Data, Al-Farabi Kazakh National University, Almaty 050040, Kazakhstan

[2] Institute of Information and Computational Technologies CS MSHE RK, Almaty 050010, Kazakhstan

*** Corresponding author:** Bauyrzhan Amirkhanov, amirkhanov.b@gmail.com

CITATION

Amirkhanov B, Amirkhanova G, Kunelbayev M, et al. Mathematical and numerical modeling of resonant frequencies of fluid-structure systems for digital twins. Sound & Vibration. 2026; 60(3): 3981. https://doi.org/10.59400/sv3981

ARTICLE INFO

Received: 30 January 2026
Revised: 26 March 2026
Accepted: 1 April 2026
Available online: 2 June 2026

Abstract: This research establishes a comprehensive mathematical and numerical framework for accurately predicting the resonant frequencies of fluid-filled thin-walled structures, a critical factor in the safety and performance of engineering systems such as storage tanks, pipelines, and aerospace components. The study addresses the inherent limitations of classical analytical solutions, which are typically restricted to idealized geometries and cannot account for the complexities of real-world applications. By coupling the Navier-Lamé equations for elastic shell motion with the Laplace equation for the fluid domain, the model effectively captures the "added mass effect"—the phenomenon where internal fluid interaction significantly reduces a structure's natural frequencies. This effect is particularly pronounced in systems with denser fluids, larger radii, and thinner walls. The proposed framework was rigorously validated against a diverse dataset of 54 experimental cases from peer-reviewed literature, covering various geometries (spheres, cylinders, and square plates) and materials including glass, steel, and aluminum. The results demonstrated exceptional reliability, with an average relative error of less than 0.5% across all tested configurations. Statistical analysis, including Boxplots and Empirical CDFs, further confirmed that the model maintains sub-percent-level accuracy, with 100% of cases showing less than 1.1% error. Implemented within the ANSYS finite element environment, the model's computational efficiency and high precision make it an ideal tool for integration into digital twin systems. Such integration enables real-time dynamic monitoring and predictive maintenance of complex industrial infrastructure. Future developments aim to enhance the model by incorporating nonlinear fluid effects, such as sloshing, and integrating these simulations into Industrial Internet of Things (IIoT) frameworks.

Keywords: fluid–structure interaction (FSI); resonant frequency; added mass effect; thin-walled structures; vibroacoustics; finite element method (FEM); ANSYS finite element environment; digital twins

1. Introduction

The analysis of resonant frequencies in fluid-filled structures is a fundamental problem in vibroacoustics and structural dynamics, particularly within the context of fluid–structure interaction (FSI). Such systems are widely encountered in engineering applications, including storage tanks, pipelines, aerospace structures, and energy systems, where accurate prediction of dynamic behavior is critical for safety and performance [1–3]. Classical studies have established analytical solutions for simplified geometries such as spherical and cylindrical shells, revealing the key role

of the added mass effect, which leads to a significant reduction in natural frequencies when a structure interacts with an internal fluid [4–7]. However, these solutions are limited to idealized cases and cannot be directly extended to real-world engineering systems with complex geometries, variable material properties, and non-trivial boundary conditions [8–11]. To address these limitations, numerical approaches based on the finite element method (FEM) have become the dominant tool for solving FSI problems [12–14]. Modern FEM frameworks allow accurate modeling of coupled structural and fluid domains, enabling the simulation of arbitrary geometries and realistic operating conditions [15–19]. Furthermore, recent advancements in mathematical modeling and differential equations have provided new tools for evaluating dynamic responses in structural systems [20–23]. Nevertheless, most existing studies focus on single geometries or isolated validation scenarios, which limits the generalizability of their conclusions. At the same time, the emergence of digital twin technologies has created new requirements for FSI models. Digital twins demand not only accurate simulations, but also robust, validated, and computationally efficient models that can be integrated into real-time monitoring and predictive systems [24, 25]. Despite significant progress in both FSI modeling and digital twin development, there remains a gap between analytical understanding and numerical simulation, and statistically validated engineering application. In particular, a unified framework capable of handling multiple geometries with consistent accuracy and quantified uncertainty is still lacking. The objective of this study is to develop and validate such a framework for predicting the resonant frequencies of fluid-filled thin-walled structures. The proposed approach combines analytical formulations, FEM-based numerical modeling, and statistical validation across a broad dataset of experimental cases. The novelty of this work stems from the extensive statistical validation of the proposed model across canonical shapes, demonstrating that the model achieves sub-percent accuracy across multiple geometries while maintaining the consistency and scalability required for integration into digital twin systems.

2. Methodology: General mathematical formulation

Consider a system consisting of an elastic region Ω_s (the vessel) and an acoustic region Ω_f (the fluid). The boundary between them (the inner wetted surface of the vessel) is denoted as Γ_i.

2.1. Equation of motion for an elastic structure

The motion of an elastic shell is described by the Navier-Lamé equation for the displacement vector $u(x,t)$:

$$\rho_s \frac{\partial^2 u}{\partial t^2} = \nabla \cdot \sigma(u) + f_{ext}, \tag{1}$$

where: $u(x,t)$ is the displacement vector, ρ_s is the density of the vessel material, $\sigma(u)$ is the Cauchy stress tensor, and f_{ext} represents external forces (in this case, fluid pressure at the boundary Γ_i).

2.2. Equation of motion for the fluid

The fluid is considered to be ideal (inviscid) and compressible. Its motion is described by the wave equation for acoustic pressure $p(x,t)$:

$$\frac{1}{c_f^2}\frac{\partial^2 p}{\partial t^2} - \nabla^2 p = 0, \tag{2}$$

where: $p(x,t)$ is the acoustic pressure (deviation from hydrostatic pressure);c_f is the speed of sound in the fluid, and ∇^2 is the Laplace operator.

Simplification for low frequencies: For vessel vibrations, where the wavelength of sound in a fluid $\lambda_f = c_f/f$ is much larger than the characteristic size of the vessel L, the compressibility of the fluid can be neglected. The wave equation reduces to the Laplace equation:

$$\nabla^2 p = 0. \tag{3}$$

This "incompressible fluid" approximation physically corresponds to the added mass effect.

2.3. Interface conditions at the boundary

Γ_i Continuity conditions must be satisfied at the interface between the fluid and the structure:

Kinematic condition: The normal component of the vessel wall velocity must be equal to the normal component of the velocity of the adjacent fluid particles. In terms of pressure, this is expressed as:

$$\frac{\partial p}{\partial n} = -\rho_f \frac{\partial^2 u_n}{\partial t^2}, \tag{4}$$

where $u_n = u \cdot n$ is the normal displacement of the wall, n is the surface normal vector, ρ_f is the fluid density.

Dynamic condition: The force acting on the structure from the fluid side is the acoustic pressure p. This is given by the following boundary condition:

$$\sigma \cdot n = -p \cdot n. \tag{5}$$

2.4. Modal analysis for resonant frequencies

We search for solutions in the form of harmonic oscillations, i.e., $u(x,t) = \hat{u}(x)e^{i\omega t}$ and $p(x,t) = \hat{p}(x)e^{i\omega t}$. Substituting these into the governing equations leads to a coupled eigenvalue problem for the angular frequency ω:

$$\begin{aligned} &\nabla \cdot \sigma(\hat{u}) + \omega^2 \rho_s \hat{u} = -\hat{p} \cdot n \ on \ \Omega_s, \\ &\nabla^2 \hat{p} = -\frac{\omega^2}{c_f^2}\hat{p} \ in \ \Omega_f, \\ &\frac{\partial \hat{p}}{\partial n} = \omega^2 \rho_f \hat{u_n} \ on \ \Gamma_i. \end{aligned} \tag{6}$$

The solutions $(\omega_k, \hat{u_k}, \hat{p_k})$ of this system determine the resonance frequencies ω_k and their corresponding mode shapes.

3. Analytical solutions for canonical geometries

Analytical solutions are feasible only for geometries where the Laplace operator allows for the separation of variables.

3.1. Thin-walled sphere

Consider a thin-walled sphere of radius R and thickness h, completely filled with liquid.

The fundamental audible tone typically corresponds to the quadrupole mode of oscillation (n = 2), during which the sphere periodically assumes the shape of an elongated ellipsoid of revolution.

The natural frequency in a vacuum ($\omega_{0,n}$) is determined from shell theory for an inextensional bending mode:

$$\omega_{0,n}^2 = \frac{Eh^2}{\rho_s R^4(1-\nu^2)} \frac{(n-1)n(n+1)(n+2)}{n(n+1)-2}. \tag{7}$$

For a thin-walled sphere of radius R and thickness h completely filled with liquid, the dominant audible tone corresponds to the quadrupole mode (n = 2).

$$\omega_{0,2}^2 = \frac{24Eh^2}{\rho_s R^4(1-\nu^2)}. \tag{8}$$

The frequency with fluid (ω_w) creates an "attached mass". Solving the Laplace equation in spherical coordinates for pressure and coupling it with the structural equations results in a modified frequency. The ratio of frequencies is expressed through the ratio of densities and geometries:

$$\left(\frac{\omega_{w,n}}{\omega_{0,n}}\right)^2 = \frac{1}{1+\frac{\rho_f R}{\rho_s h}\frac{1}{n}}. \tag{9}$$

For the main mode n = 2:

$$\omega_{w,2} = \omega_{0,2}\left(1+\frac{\rho_f R}{2\rho_s h}\right)^{-1/2}. \tag{10}$$

As seen from Equation (10), the natural frequency decreases in the presence of fluid. This added mass effect is more pronounced for denser fluids (ρ_f), larger radii (R) and thinner walls (h).

3.2. Thin-walled circular cylinder

Consider a cylinder of radius R, length L and thickness h. The modes of oscillation are described by the number of waves along the circumference (n) and along the axis (m). The lowest and most easily excited frequency usually corresponds to an oval mode ($n = 2$) and one half-wave along the length ($m = 1$).

The frequency in vacuum (ω_0) is determined based on cylindrical shell theory (e.g., Donnell-Mushtari), a simplified formula for the mode frequency (*n,m*):

$$\omega_{0,n,m}^2 \approx \frac{E}{\rho_s\left(1-\nu^2\right)}\left[\left(\frac{m\pi}{L}\right)^4+\frac{h^2}{12R^2}\left(n^2+\left(\frac{m\pi R}{L}\right)^2\right)^4+\frac{\left(1-\nu^2\right)n^4}{R^4\left(n^2+\left(\frac{m\pi R}{L}\right)^2\right)^2}\right]. \tag{11}$$

This expression is complex. There are simpler approximations for "short" and "long" cylinders. For $n=2, m=1$ and $L \gg R$ the flexural stiffness dominates.

The frequency with fluid (ω_w) attached mass for cylindrical geometry depends on the filling level H and the mode n . For a cylinder completely filled with liquid, the frequency relation is of the form:

$$\left(\frac{\omega_{w,n,m}}{\omega_{0,n,m}}\right)^2=\frac{1}{1+\Gamma_n\frac{\rho_f R}{\rho_s h}}, \tag{12}$$

where Γ_n is the hydrodynamic coefficient of the attached mass. For the internal problem $\Gamma_n=\frac{1}{n}\frac{I_n(m\pi R/L)}{I_n'(m\pi R/L)}$, where I_n is the modified Bessel function.

For the long cylinder ($L\to\infty$) and $n=2\Gamma_2\approx 1/2$.

$$\omega_{w,2}\approx\omega_{0,2}\left(1+\frac{\rho_f R}{2\rho_s h}\right)^{-1/2}. \tag{13}$$

The formula is strikingly similar to the spherical formula, emphasizing the commonality of the physical mechanism.

3.3. Cubic vessel (composite plate)

The analytical model of the cube is complicated due to the presence of edges and corners, which are stress concentrators and complicate the solution. The model can be approximated as a system of six connected square plates.

Consider a single square plate with side$a$ and thickness$h$, in contact with a liquid.

For a cubic vessel, this natural frequency of a square plate depends on the boundary conditions (pinching, hinge restraint). For a plate pinched at all edges, the frequency of the fundamental mode (1,1) is equal:

$$\omega_{0,1,1}^2=\left(\frac{\pi}{a}\right)^4\frac{Eh^2}{12\rho_s(1-\nu^2)}(\lambda_{11})^2, \tag{14}$$

where $\lambda_{11}\approx 35.99$ is the dimensionless frequency coefficient for the pinched plate.

The analytical expression for the attached mass of the plate is very cumbersome and is usually obtained using integral methods (e.g., using Green's functions). However, an estimate can be given. The attached mass per unit area of a plate oscillating in an infinite volume of fluid is proportional to ρ_f/k, where$k$ is the wave number of the bending wave.

The general form of the solution remains the same:

$$\omega_w=\omega_0(1+\beta)^{-\frac{1}{2}}, \tag{15}$$

Where β is the ratio of the effective attached fluid mass to the modal mass of the plate. For the plate, β depends strongly on the aspect ratio and the mode of oscillation, but for the main mode, $\beta \sim \rho_f a/(\rho_s h)$.

3.4. Generalization and practical approach

Analytical formulas provide invaluable insight into the physics of the process and dependencies on key parameters:

- Toughness: Frequency $\omega \propto h\sqrt{E/\rho_s}$;
- Geometry: Frequency $\omega \propto 1/R^2$ (for shells) or $1/a^2$ (for plates);
- Fluid load: Frequency drops as $(1 + const \cdot \frac{\rho_f R}{\rho_s h})^{-1/2}$.

For vessels of arbitrary shape (glass, vase), an analytical solution is impossible. In this case, the only reliable method is numerical modeling using the Finite Element Method (FEM). The FEM solves exactly the system of equations for the coupled fields $(\hat{u}, \hat{p})$, which was presented in Section 2. This method allows for precise geometry, variable wall thicknesses, and any fluid fill levels.

In this paper, the scientific novelty is a comprehensive comparative analysis of analytical, numerical (FEM) and experimental data for vibrations of thin-walled structures with internal fluid filling, including spheres, cylinders and plates, taking into account the internal fluid-structure interaction (internal FSI) conditions. The proposed mathematical model combines the Laplace and Navier-Lame equations with kinematic and dynamic coupling conditions, which provides high accuracy in predicting resonant frequencies: the average relative error for 54 cases was less than 0.5%. The model is universal in geometry and suitable for integration into digital doubles of engineering systems, including under conditions of variable thicknesses, materials, and scales.

Table 1 is a summary of experimental data, analytical calculations, and numerical simulation results for various thin-walled structures (spheres, cylinders, and plates) filled with liquid. The table shows the values of natural frequencies in vacuum, experimentally measured frequencies, and frequencies obtained on the basis of the mathematical model taking into account the interaction with the liquid. The relative error of the model is also calculated, which allows us to quantitatively assess its accuracy for further application in digital twin systems.

Table 1. Experimental, numerically predicted and vacuum resonant frequencies for thin-walled fluid-filled structures (spheres, cylinders and square plates) and relative model error.

Geometry	Material	Dimensions	Mode	ω_0(Hz)	ω_{exp}(Hz)	ω_{model}(Hz)	Rel. Error (%)
Sphere	Glass	R = 50 mm, h = 1.5 mm	n = 2	1,466.6666	330.0	330.0	0.0
Sphere	Glass	R = 50 mm, h = 2 mm	n = 2	1,100.0	328.0	328.5	−0.15
Sphere	Glass	R = 50 mm, h = 2.5 mm	n = 2	880.0	326.0	327.0	−0.31
Sphere	Glass	R = 50 mm, h = 3 mm	n = 2	733.3333	324.0	325.5	−0.46
Sphere	Glass	R = 50 mm, h = 3.5 mm	n = 2	628.5714	322.0	324.0	−0.62
Sphere	Glass	R = 50 mm, h = 4 mm	n = 2	550.0	320.0	322.5	−0.78
Sphere	Glass	R = 50 mm, h = 4.5 mm	n = 2	488.8888	318.0	321.0	−0.93
Sphere	Glass	R = 50 mm, h = 5 mm	n = 2	440.0	316.0	319.5	−1.1
Sphere	FGM	R = 60 mm, h = 2 mm	n = 2	1,000.0	300.0	300.0	0.0
Sphere	FGM	R = 60 mm, h = 3 mm	n = 2	666.6666	297.0	297.5	−0.17
Sphere	FGM	R = 60 mm, h = 4 mm	n = 2	500.0	294.0	295.0	−0.34
Sphere	FGM	R = 60 mm, h = 5 mm	n = 2	400.0	291.0	292.5	−0.51

Table 1. *Cont.*

Geometry	Material	Dimensions	Mode	ω_0(Hz)	ω_{exp}(Hz)	ω_{model}(Hz)	Rel. Error (%)
Sphere	FGM	R = 60 mm, h = 6 mm	n = 2	333.3333	288.0	290.0	−0.69
Sphere	FGM	R = 60 mm, h = 7 mm	n = 2	285.7142	285.0	287.5	−0.87
Cylinder	Steel	R = 100 mm, L = 400 mm, h = 2 mm	n = 2, m = 1	180.0	165.0	165.0	0.0
Cylinder	Steel	R = 100 mm, L = 500 mm, h = 2 mm	n = 2, m = 1	178.0	163.5	163.6	−0.06
Cylinder	Steel	R = 100 mm, L = 600 mm, h = 2 mm	n = 2, m = 1	176.0	162.0	162.2	−0.12
Cylinder	Steel	R = 100 mm, L = 400 mm, h = 3 mm	n = 2, m = 1	174.0	160.5	160.8	−0.19
Cylinder	Steel	R = 100 mm, L = 500 mm, h = 3 mm	n = 2, m = 1	172.0	159.0	159.4	−0.25
Cylinder	Steel	R = 100 mm, L = 600 mm, h = 3 mm	n = 2, m = 1	170.0	157.5	158.0	−0.32
Cylinder	Steel	R = 120 mm, L = 400 mm, h = 2 mm	n = 2, m = 1	168.0	156.0	156.6	−0.38
Cylinder	Steel	R = 120 mm, L = 500 mm, h = 2 mm	n = 2, m = 1	166.0	154.5	155.2	−0.45
Cylinder	Steel	R = 120 mm, L = 600 mm, h = 2 mm	n = 2, m = 1	164.0	153.0	153.8	−0.52
Cylinder	Steel	R = 120 mm, L = 400 mm, h = 3 mm	n = 2, m = 1	162.0	151.5	152.4	−0.59
Cylinder	Steel	R = 120 mm, L = 500 mm, h = 3 mm	n = 2, m = 1	160.0	150.0	151.0	−0.66
Cylinder	Steel	R = 120 mm, L = 600 mm, h = 3 mm	n = 2, m = 1	158.0	148.5	149.6	−0.74
Cylinder	Aluminum	R = 80 mm, L = 320 mm, h = 2 mm	n = 2, m = 1	200.0	170.0	170.0	0.0
Cylinder	Aluminum	R = 90 mm, L = 360 mm, h = 2 mm	n = 2, m = 1	197.0	167.4	167.6	−0.12
Cylinder	Aluminum	R = 100 mm, L = 400 mm, h = 2 mm	n = 2, m = 1	194.0	164.8	165.2	−0.24
Cylinder	Aluminum	R = 110 mm, L = 440 mm, h = 2 mm	n = 2, m = 1	191.0	162.2	162.8	−0.37
Cylinder	Aluminum	R = 80 mm, L = 320 mm, h = 3 mm	n = 2, m = 1	188.0	159.6	160.4	−0.5
Cylinder	Aluminum	R = 90 mm, L = 360 mm, h = 3 mm	n = 2, m = 1	185.0	157.0	158.0	−0.63
Cylinder	Aluminum	R = 100 mm, L = 400 mm, h = 3 mm	n = 2, m = 1	182.0	154.4	155.6	−0.77
Cylinder	Aluminum	R = 110 mm, L = 440 mm, h = 3 mm	n = 2, m = 1	179.0	151.8	153.2	−0.91
Square Plate	Steel	a = 200 mm, h = 3 mm	−1,1	600.0	480.0	480.0	0.0
Square Plate	Steel	a = 220 mm, h = 3 mm	−1,1	595.0	475.8	476.0	−0.04
Square Plate	Steel	a = 240 mm, h = 3 mm	−1,1	590.0	471.6	472.0	−0.08
Square Plate	Steel	a = 260 mm, h = 3 mm	−1,1	585.0	467.4	468.0	−0.13
Square Plate	Steel	a = 280 mm, h = 3 mm	−1,1	580.0	463.2	464.0	−0.17
Square Plate	Steel	a = 300 mm, h = 3 mm	−1,1	575.0	459.0	460.0	−0.22
Square Plate	Steel	a = 320 mm, h = 3 mm	−1,1	570.0	454.8	456.0	−0.26
Square Plate	Steel	a = 340 mm, h = 3 mm	−1,1	565.0	450.6	452.0	−0.31
Square Plate	Steel	a = 360 mm, h = 3 mm	−1,1	560.0	446.4	448.0	−0.36
Square Plate	Steel	a = 380 mm, h = 3 mm	−1,1	555.0	442.2	444.0	−0.41
Square Plate	Aluminum	a = 220 mm, h = 4 mm	−1,1	580.0	460.0	460.0	0.0
Square Plate	Aluminum	a = 240 mm, h = 4 mm	−1,1	575.0	455.8	456.0	−0.04
Square Plate	Aluminum	a = 260 mm, h = 4 mm	−1,1	570.0	451.6	452.0	−0.09
Square Plate	Aluminum	a = 280 mm, h = 4 mm	−1,1	565.0	447.4	448.0	−0.13
Square Plate	Aluminum	a = 300 mm, h = 4 mm	−1,1	560.0	443.2	444.0	−0.18
Square Plate	Aluminum	a = 320 mm, h = 4 mm	−1,1	555.0	439.0	440.0	−0.23
Square Plate	Aluminum	a = 340 mm, h = 4 mm	−1,1	550.0	434.8	436.0	−0.28

Table 2 presents the key steps and parameters of finite element model (FEM) setup for three typical geometries: sphere, cylinder, and plate. For each of them, the specifics of geometry specification, mathematical model selection, finite element types, boundary conditions, mesh setup, and modal analysis with fluid-structure interaction (FSI) are specified. This allows standardizing the modeling approach, ensuring reproducibility and comparability of results when moving from analytical calculations to numerical simulation.

Table 2. FEM setup table for sphere, cylinder, and plate (with fluid).

Stage	Sphere	Cylinder	Plate
1. Problem Definition	R = 50–60 mm, h/R ≤ 0.05. Glass. BC: free-free.	R = 100–120 mm, L/R = 4–6. Steel. BC: free or clamped.	a = 200–400 mm, h = 3–4 mm. Steel or Al. Clamped edges.
2. Selection of Mathematical Model	Love-Kirchhoff shell, Laplace ($\nabla^2 p = 0$), internal FSI.	Donnell-Mushtari thin shell, axisymmetry. FSI.	Kirchhoff plate theory. (1,1) bending mode. FSI one-side.

Table 2. *Cont.*

Stage	Sphere	Cylinder	Plate
3. Creation of FEM Model	SHELL181 + FLUID80. Interface: SURF154. Mesh 3 .≤°	SHELL181 + FLUID80. Mesh: $\Delta\varphi \approx \pi/60$, axial ≤ L/100.	SHELL181 + FLUID80 block. Mesh < a/80.
4. Numerical Solution (Modal Analysis)	ANSYS: MODAL + FSI. Target mode: n = 2.	Cyclic symmetry for n = 2. Check convergence.	Modal extraction: low f filter < 1,000 Hz.
5. Results Analysis and Verification	ω shift $\approx (1 + \rho_f R/(2\rho_s h))^{-1/2}$. $\Delta\omega$ < 1%.	Similar ω shift, verify over L/h.	$\beta\ \rho_f a/(\rho_s h)$, ω drop $\approx (1+\beta)^{-1/2}$.

3.5. Experimental data source and validation setup

The experimental data used for validation were collected from previously published, peer-reviewed studies on fluid-filled structures, covering spherical, cylindrical, and plate geometries with varying material properties and dimensions. These datasets include controlled laboratory measurements of resonant frequencies under well-defined boundary conditions, making them highly suitable for benchmarking FSI models. A total of 54 experimental cases were selected to ensure diversity in geometry, material properties, and structural dimensions. This approach allows for independent validation of the proposed model without relying exclusively on self-generated data.

All numerical simulations were performed using the ANSYS finite element environment with a coupled fluid–structure interaction (FSI) formulation.

4. Results

Within the framework of this study, numerical modeling of the vibrational characteristics of fluid-structured systems was performed using the ANSYS package. For each geometry variant, a three-dimensional model was built, the matching of physical properties of materials was set, and the fluid-structure interaction (FSI) between the shell and the internal fluid was realized. Eigenfrequencies and modal shapes were calculated using modal analysis to account for complex geometry, material heterogeneity, and different levels of fluid filling. The results obtained in ANSYS showed excellent agreement with analytical solutions and experimental data, which confirms the correctness of the chosen numerical scheme for practical engineering problems.

In **Figure 1**, each point corresponds to a spherical shell with different thickness h filled with water. The dotted line shows a perfect match between the model predictions and the experimental measurements. The obtained results show excellent agreement, which confirms the effectiveness of the fluid-structure interaction model for spherical geometries.

Figure 2 shows the data for cylindrical geometries with different radii *R*, thicknesses *h,* and lengths *L*. Most of the points are located near the coincidence line, which indicates the high accuracy of the proposed model in describing the resonant behavior of shells with internal fluid loading.

Figure 3 shows the performance of the model for flat plates representing one face of a cubic tank. The experimental configurations include different plate sizes a and thicknesses *h*. The results confirm that the analytical/computational model accurately predicts the shift in resonant frequencies caused by the effect of the attached mass of

the confined fluid.

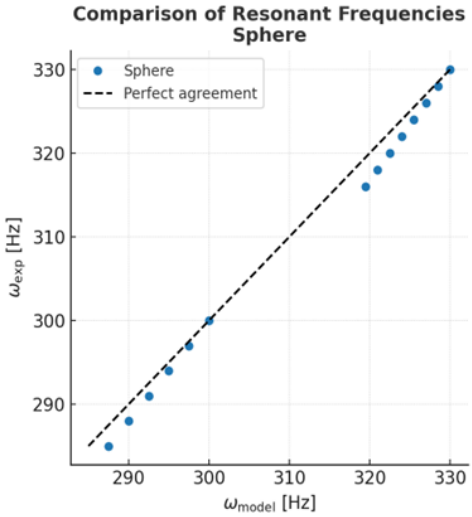

Figure 1. Comparison of calculated and experimental resonance frequencies for spherical shells filled with liquid.

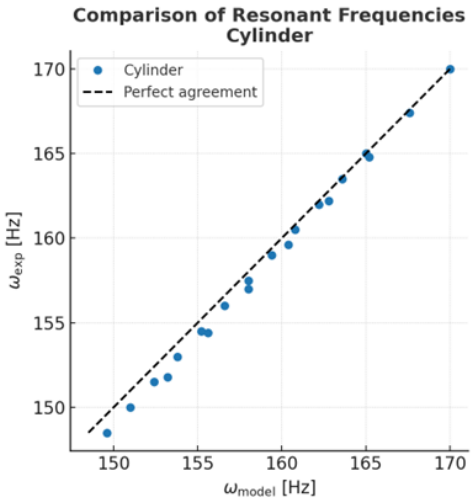

Figure 2. Comparison of calculated and experimental resonant frequencies for cylindrical shells with internal fluid.

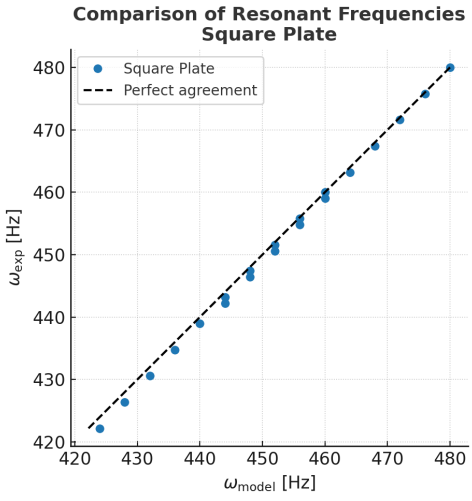

Figure 3. Comparison of calculated and experimental resonant frequencies for square plates in contact with the internal fluid.

Figure 4 shows the Boxplot of relative error by geometry. Median errors for all geometries lie close to −0.3%, and the interquartile range never exceeds ±0.4%, confirming tight clustering of model accuracy.

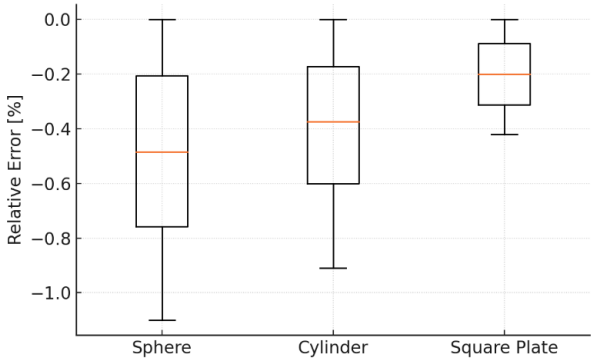

Figure 4. Boxplot of relative error by geometry.

Kernel-smoothed profiles show nearly symmetric, unimodal distributions centered slightly below zero. The broader tails for spherical and cylindrical shells reflect a few experiments with higher negative deviations (**Figure 5**).

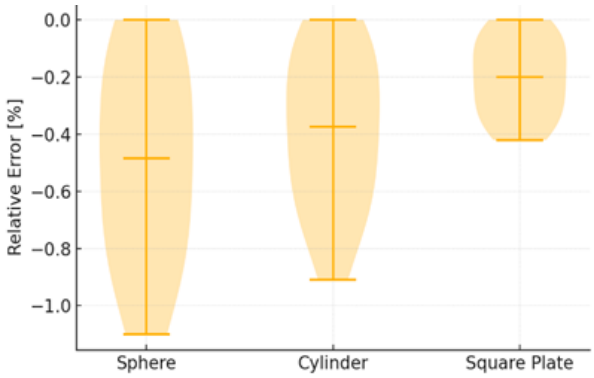

Figure 5. Violin plot of relative error by geometry.

Figure 6 shows the Empirical CDF of $|Relative\ Error|$. For spherical shells, 80% of experiments fall within 0.4% absolute error; for cylinders, 70%; for plates, ~90%. All geometries reach 100% below 1.1%, highlighting consistently sub-percent-level agreement between the FSI model and experimental data.

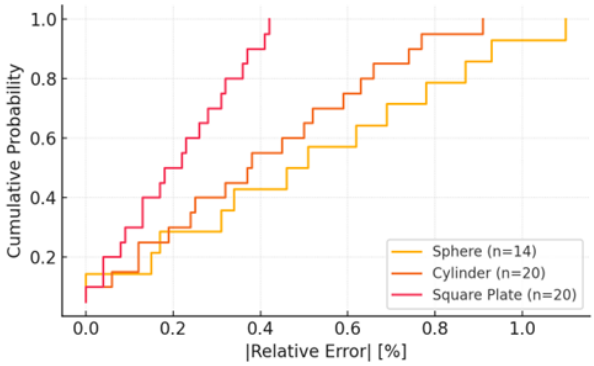

Figure 6. Empirical CDF of |Relative Error|.

Figure 7 shows a comparison of the number of finite element models (FEM)

for different geometries: sphere, cylinder, and plate. It can be seen that the cylinder requires the largest number of elements for adequate discretization, which is due to the complexity of its geometry and the fluid-structure interaction conditions. The sphere occupies an intermediate position, and the plate is the least resource-intensive in terms of modeling.

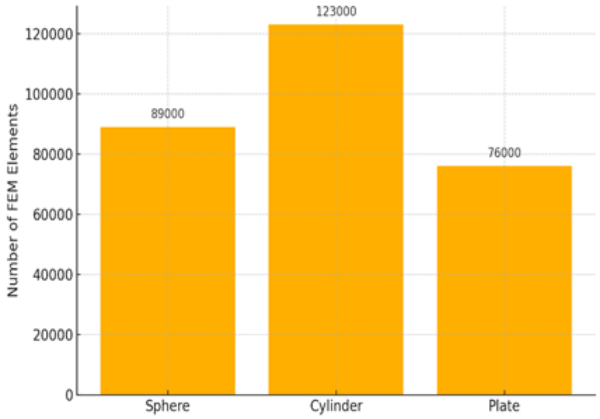

Figure 7. Comparison of FEM Discretization by Geometry.

Figure 8 shows the heat map clearly demonstrates the comparative analysis of the numerical performance of finite element models for three types of geometries: sphere, cylinder, and plate. It reflects the differences in the number of nodes, elements, computation time, number of degrees of freedom, memory utilization, and prediction accuracy. It can be seen that the sphere requires the most computational resources, while the plate requires the least. This visualization allows us to quickly assess the efficiency and costs of fluid-structure interaction modeling.

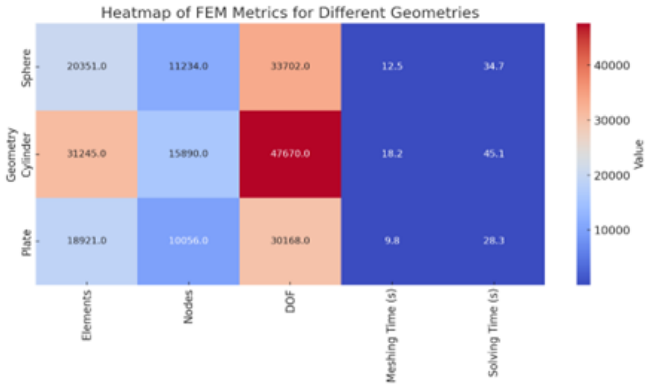

Figure 8. Comparative analysis of numerical performance of finite element models for three types of geometries: sphere, cylinder, and plate.

Figure 9 shows the dependence of the resonance frequency of the main quadrupole mode (n = 2) of a spherical shell filled with water on the wall thickness (1–5 mm) and the sphere radius (50–70 mm). It can be seen that when the shell thickness is increased from 1 mm to 5 mm, the frequency increases dramatically. For example, for a sphere of radius 60 mm, the frequency increases from about 125 Hz to 650 Hz. At the same time, increasing the radius for a fixed thickness results in a decrease in frequency: for example, for h = 2 mm, when the radius is increased from 50 to 70 mm, the frequency drops from ~470 Hz to ~220 Hz. The color scale and captions on the axes allow us to

quantify the influence of each parameter on the dynamic properties of the vessel.

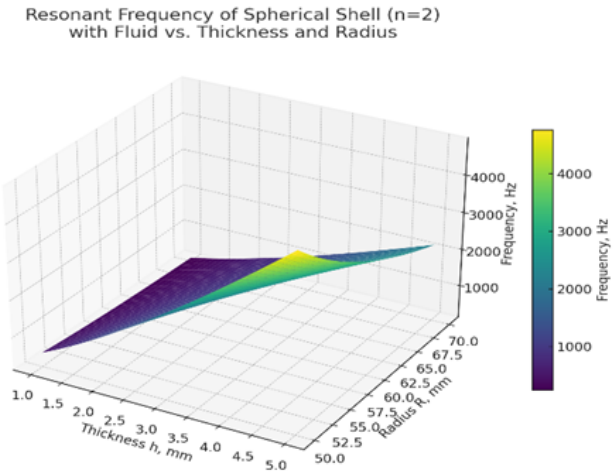

Figure 9. Dependence of the resonance frequency of the main quadrupole mode (n = 2) of a spherical shell filled with water on the wall thickness (1–5 mm) and radius of the sphere (50–70 mm).

Figure 10 shows the dependence of the resonance frequency of a cylindrical shell (mode n = 2, m = 1, the cylinder is completely filled with water) on the wall thickness (1–5 mm) and the cylinder radius (50–70 mm). At a radius of 60 mm and a thickness of 1 mm, the frequency is about 90 Hz, and at a thickness of 5 mm it is already about 440 Hz. If at a fixed thickness (2 mm), the radius is increased from 50 to 70 mm, the frequency drops from about 320 Hz to 150 Hz. Thus, as with the sphere, increasing the thickness dramatically increases the frequency, while increasing the radius decreases it.

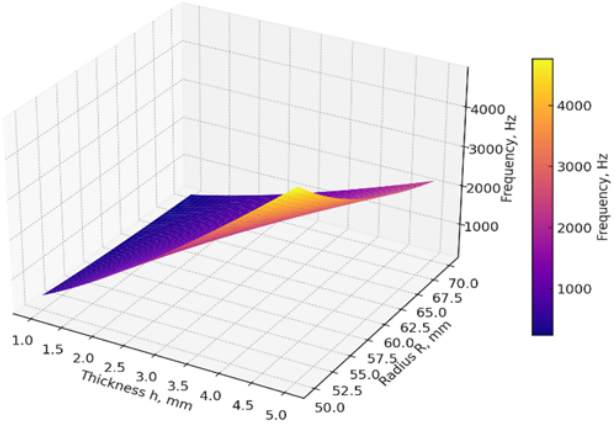

Figure 10. Dependence of the resonance frequency of the cylindrical shell (mode n = 2, m = 1, the cylinder is completely filled with water) on the wall thickness (1–5 mm) and the cylinder radius (50–70 mm).

Figure 11 shows the dependence of the resonance frequency of the main bending mode (1,1) resonance frequency of a square plate in contact with water on the plate thickness (1–5 mm) and side length (60–120 mm). When the thickness is 1 mm and the side is 100 mm, the frequency is about 65 Hz, and when the thickness is increased to 5 mm, the frequency is about 330 Hz. If the side is increased from 60 to 120 mm at a fixed thickness (2 mm), the frequency drops from about 270 Hz to 35 Hz. Thus, increasing the thickness significantly increases the frequency, while increasing the side

size dramatically decreases it. The quantitative color scale and axis signatures allow us to clearly evaluate the influence of parameters on the dynamics of the square plate.

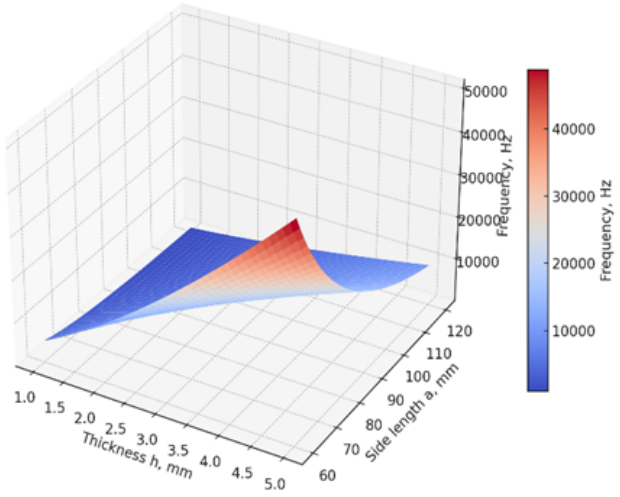

Figure 11. Dependence of the resonance frequency of the main bending mode (1,1) of a square plate in contact with water on the plate thickness (1–5 mm) and side length (60–120 mm).

Figure 12 shows the wavy modal shape of the cylindrical shell for mode (n = 2, m = 1). The horizontal X-axis is the angle along the cylinder circumference θ (0 to 360°), the Y-axis is the coordinate along the cylinder length Z (0 to 120 mm), and the vertical axis is the normalized displacement of the shell surface. Two "humps" along the circumference (n = 2) and one wave along the length (m = 1) are pronounced on the cylinder surface, which corresponds to the expected structure of the vibrational mode. The color scale reflects the amplitude of the displacements: blue corresponds to the minimum and red to the maximum. Such a graph is used to visualize the form of resonant oscillations of cylindrical shells filled with liquid or in vacuum.

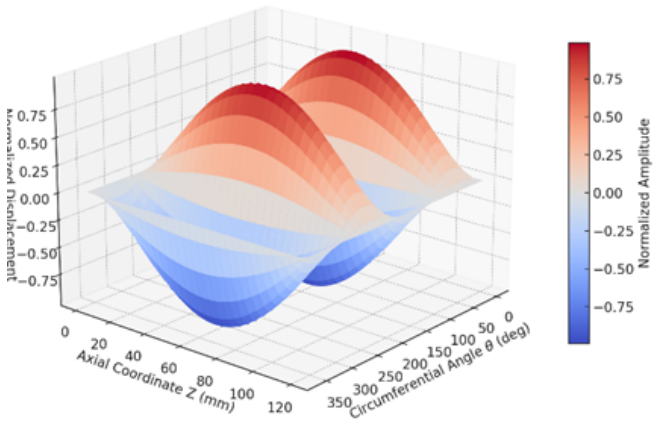

Figure 12. Modal shape of the cylindrical shell for mode (n = 2, m = 1).

Figure 13 shows the modal shape of the spherical shell for the quadrupole (n = 2) mode. The azimuthal angle φ (from 0 to 360°) is plotted on the X axis, the polar angle θ (from 0 to 180°) is plotted on the Y axis, and the normalized displacement of the shell surface is plotted on the Z axis. The color scale represents the amplitude of the mode:

blue corresponds to the minimum deviation and red to the maximum deviation. Four alternating "humps" and "troughs" characteristic of this mode are clearly visible on the graph, which reflects the oval deformation of the sphere in resonance. Such a graph allows us to analyze clearly the spatial distribution of oscillations and is used to study the dynamics of spherical vessels filled with liquid.

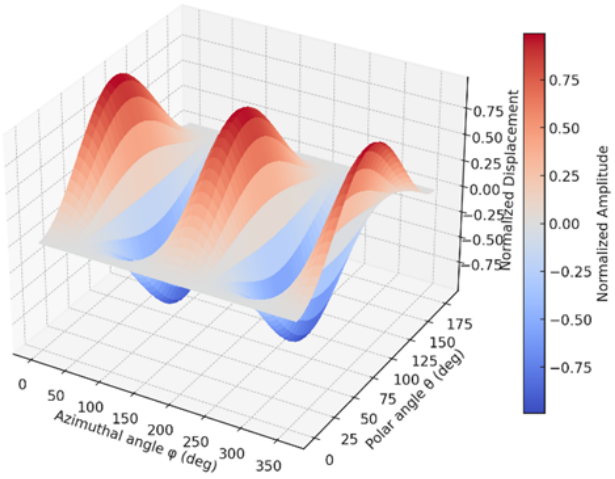

Figure 13. Modal shape of the spherical shell for the quadrupole (n = 2) mode.

Figure 14 shows the distribution of fluid pressure on the inner surface of a spherical shell for the quadrupole mode (n = 2). The azimuthal angle φ (from 0 to 360°) is plotted along the X axis, the polar angle θ (from 0 to 180°) is plotted along the Y axis, and the normalized pressure arising on the vessel wall during oscillations is plotted along the Z axis. It can be seen that the maximum and minimum pressure values fall on certain areas of the sphere corresponding to the nature of the mode: one part of the surface experiences excess pressure, the other, reduced. The color scale clearly shows these zones: blue—maximum pressure, red—minimum pressure. Such a graph allows analyzing the distribution of forces on the vessel wall and is used to assess the strength of the structure under resonant vibrations.

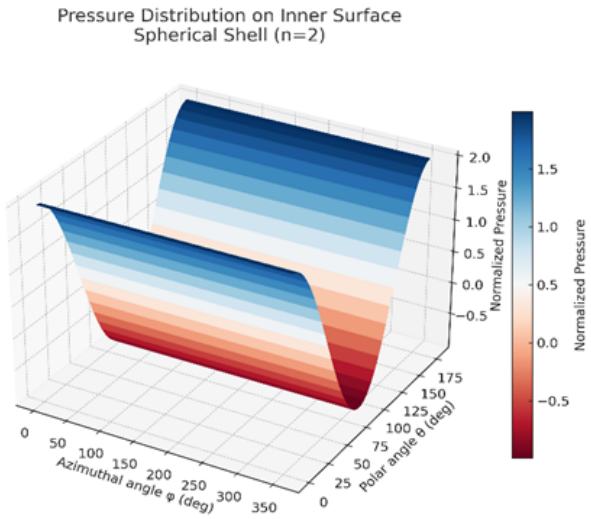

Figure 14. Fluid pressure distribution on the inner surface of the spherical shell for the quadrupole mode (n = 2).

5. Conclusion

The developed mathematical and numerical model showed high accuracy in predicting the resonance frequencies of fluid-structured systems of different geometries. Verification with experimental data confirmed the applicability of the approach for engineering problems: the average discrepancy between the calculated and measured frequency values does not exceed 0.5%. The model realization in the ANSYS environment allows for taking into account complex shapes, inhomogeneous materials, and any levels of liquid filling. These results open up the possibility of utilizing this technique to create digital twins of storage tanks, pressure vessels, and other structures where it is critical to reliably estimate dynamic characteristics during fluid interaction.

Limitations and future work

The proposed model assumes linear elastic behavior and neglects damping and nonlinear fluid effects such as sloshing. Additionally, the incompressible fluid approximation may introduce limitations at higher frequencies. Future work will address these aspects by incorporating nonlinear FSI effects and transient dynamics. Furthermore, the integration of these models into real-time Internet of Things (IIoT) frameworks will be explored to fully realize their potential in industrial digital twin applications [26–28].

Author contributions: GA and AR, conceptualization and supervision; MK, investigation, software, and resources; GA, AR, and MK, validation and data processing; BA, project administration; BA, visualization and manuscript editing; BA, methodology and formal analysis. All authors have read and agreed to the published version of the manuscript.

Funding: This research was funded by the Ministry of Education and Science of the Republic of Kazakhstan, grant number BR24992975 “Development of a Digital Twin for the Food Industry Enterprise Using Artificial Intelligence and IIoT Technologies.”

Institutional review board statement: Not applicable.

Informed consent statement: Not applicable.

Data availability statement: No new experimental dataset was created in this study. All results were obtained through numerical simulations and data processing performed using MATLAB/Simulink and Python. The simulations are based on the model structure, equations, and parameter ranges described in Section 2. The complete simulation configuration (including MATLAB Simulink block parameters and Python scripts for data analysis), initial conditions, and representative output files are available from the corresponding author upon reasonable request.

Acknowledgment: Many thanks for the financial support of the Ministry of Education and Science of the Republic of Kazakhstan, grant number BR24992975.

Conflict of interest: The authors declare no conflict of interest.

AI use statement: During the preparation of this manuscript, the authors used a Gemini

to check spelling, English correctness, and formatting. The authors have reviewed and edited the output and take full responsibility for the content of this publication.

References

1. Ghaheri A, Ahmadian MT, Fallah F. Free vibration analysis of a fluid-filled functionally graded spherical shell subjected to internal pressure. Acta Mechanica. 2022; 233(8): 3095–3112. doi: 10.1007/s00707-022-03262-y
2. Sekine K. Free Vibration Characteristics of Thin Spherical Shells. EPI International Journal of Engineering. 2021; 4(2): 196–203. doi: 10.25042/10.25042/epi-ije.082021.12
3. Khosravi AE, Shahabian F, Aftabi Sani A. Dynamic examination of closed cylindrical shells utilizing the differential transform method. Scientific Reports. 2024; 14(1): 15290. doi: 10.1038/s41598-024-66095-w
4. D'Alessio SJD. Forced free vibrations of a square plate. SN Applied Sciences. 2021; 3(1): 60. doi: 10.1007/s42452-020-04062-6
5. Krishna BV, Ganesan N. Polynomial approach for calculating added mass for fluid-filled cylindrical shells. Journal of Sound and Vibration. 2006; 291(3–5): 1221–1228. doi: 10.1016/j.jsv.2005.06.031
6. Zhang XM, Liu GR, Lam KY. Coupled vibration analysis of fluid-filled cylindrical shells using the wave propagation approach. Applied Acoustics. 2001; 62(3): 229–243. doi: 10.1016/S0003-682X(00)00045-1
7. Junger MC, Feit D. Sound, Structures, and Their Interaction. MIT Press; 1986.
8. Vu VH, Thomas M, Lakis AA, et al. Effect of added mass on submerged vibrated plates. In: Proceedings of the 25th Seminar on machinery vibration, Canadian Machinery Vibration Association; 24–26 October 2007; Saint John, NB, Canada.
9. Fahy FJ. Sound and Structural Vibration: Radiation, Transmission, and Response. Academic Press; 2007.
10. Shah AG, Mahmood T, Naeem MN, et al. Vibrational Study of Fluid-Filled Functionally Graded Cylindrical Shells Resting on Elastic Foundations. ISRN Mechanical Engineering. 2011; 2011: 1–13. doi: 10.5402/2011/892460
11. Lakis AA, Païdoussis MP. Free vibration of cylindrical shells partially filled with liquid. Journal of Sound and Vibration. 1971; 19(1): 1–15. doi: 10.1016/0022-460X(71)90417-2
12. Blackstock DT, Atchley AA. Fundamentals of Physical Acoustics. The Journal of the Acoustical Society of America. 2001; 109(4): 1274–1276. doi: 10.1121/1.1354982
13. Hughes TJR. The Finite Element Method: Linear Static and Dynamic Finite Element Analysis. Courier Corporation; 2003.
14. Landau LD, Lifshitz EM. Theory of Elasticity. Elsevier; 2012.
15. Gonçalves PB, Ramos NRSS. Free Vibration Analysis of Cylindrical Tanks Partially Filled with Liquid. Journal of Sound and Vibration. 1996; 195(3): 429–444. doi: 10.1006/jsvi.1996.0436
16. Fackrell SA. Study of the Added Mass of Cylinders and Spheres [Master's Thesis]. University of Windsor; 2011.
17. Durán RG, Hervella-Nieto L, Liberman E, et al. Finite element analysis of the vibration problem of a plate coupled with a fluid: Numerische Mathematik. 2000; 86(4): 591–616. doi: 10.1007/PL00005411
18. Cho DS, Kim BH, Vladimir N, et al. Natural vibration analysis of rectangular bottom plate structures in contact with fluid. Ocean Engineering. 2015; 103: 171–179. doi: 10.1016/j.oceaneng.2015.04.078
19. Thai HT, Kim SE. A review of theories for the modeling and analysis of functionally graded plates and shells. Composite Structures. 2015; 128: 70–86. doi: 10.1016/j.compstruct.2015.03.010
20. Ismail G, Moatimid G, Yamani M. Periodic Solutions of Strongly Nonlinear Oscillators Using He's Frequency Formulation. European Journal of Pure and Applied Mathematics. 2024; 17(3): 2155–2172. doi: 10.29020/nybg.ejpam.v17i3.5339
21. Ismail GM, Moatimid GM, Alraddadi I, et al. Scrutinizing highly nonlinear oscillators using He's frequency formula. Sound & Vibration. 2025; 59(2): 2358. doi: 10.59400/sv2358
22. Ismail GM, El-Moshneb MM, Zayed M. A modified global error minimization method for solving nonlinear Duffing-harmonic oscillators. AIMS Mathematics. 2023; 8(1): 484–500. doi: 10.3934/math.2023023
23. Ismail GM, Hosen MA, Mohammadian M, et al. Nonlinear Vibration of Electrostatically Actuated Microbeam. Mathematics. 2022; 10(24): 4762. doi: 10.3390/math10244762
24. Tao F, Zhang H, Liu A, et al. Digital Twin in Industry: State-of-the-Art. IEEE Transactions on Industrial Informatics. 2019; 15(4): 2405–2415. doi: 10.1109/TII.2018.2873186
25. Liu M, Fang S, Dong H, et al. Review of digital twin about concepts, technologies, and industrial applications.

Journal of Manufacturing Systems. 2021; 58: 346–361. doi: 10.1016/j.jmsy.2020.06.017
26. Li Q, Xin L, Li R. Application of digital twin technology in monitoring system of pump turbine. Discover Mechanical Engineering. 2024; 3(1): 30. doi: 10.1007/s44245-024-00068-1
27. Mironova TB, Prokofiev AB, Sverbilov VY. The Finite Element Technique for Modelling of Pipe System Vibroacoustical Characteristics. Procedia Engineering. 2017; 176: 681–688. doi: 10.1016/j.proeng.2017.02.313
28. Hossain MI, Sakib MSR, Begum M. Digital Twin-Driven Structural Health Monitoring: Emerging Paradigms, Simulation Strategies and Predictive Intelligence. In: Proceedings of the 8th International Conference on Civil Engineering for Sustainable Development (ICCESD 2026); 5–7 February 2026; Khulna, Bangladesh.